Self-Assembly of a Pd2L4 Hydrazone Molecular Cage Through Multiple Reaction Pathways

Giovanni Montà-González , Ramón Martínez-Máñez * , Vicente Martí-Centelles *

Posted Date: 14 October 2024

doi: 10.20944/preprints202410.1100.v1

Keywords: molecular cages; supramolecular chemistry; metal-organic cages; self-assembly

Article

Self-Assembly of a Pd_2L_4 Hydrazone Molecular Cage Through Multiple Reaction Pathways

Giovanni Montà-González, [1,2] Ramón Martínez-Máñez [1,2,3,4,5,*] and Vicente Martí-Centelles, [1,2,3,*]

[1] Instituto Interuniversitario de Investigación de Reconocimiento Molecular y Desarrollo Tecnológico (IDM), Universitat Politècnica de València, Universitat de València, Camino de Vera s/n, 46022, Valencia, Spain
[2] Departamento de Química, Universitat Politècnica de València, Camino de Vera s/n, 46022, Valencia, Spain
[3] CIBER de Bioingeniería Biomateriales y Nanomedicina, Instituto de Salud Carlos III, Spain
[4] Unidad Mixta de Investigación en Nanomedicina y Sensores, Universitat Politècnica de València, Instituto de Investigación Sanitaria La Fe (IISLAFE), Avenida Fernando Abril Martorell, 106, 46026, Valencia, Spain
[5] Unidad Mixta UPV-CIPF de Investigación en Mecanismos de Enfermedades y Nanomedicina, Universitat Politècnica de València, Centro de Investigación Príncipe Felipe, Avenida Eduardo Primo Yúfera, 3, 46012, Valencia, Spain
* Correspondence: VMC vimarce1@upv.es; RMM rmaez@qim.upv.es

Abstract: Molecular cages are preorganized molecules with a central cavity, typically formed through the self-assembly of their building blocks. This requires in most cases forming and breaking reversible bonds during the self-assembly reaction pathway for error correction to drive the reaction to the cage product. In this work, we focus on both Pd–ligand and hydrazone bonds implemented in the structure of a Pd_2L_4 hydrazone molecular cage. As the cage contains two different types of reversible bonds, we envisaged a cage formation comparative study by performing the self-assembly of the cage through 3 different reaction pathways involving the formation of Pd–ligand bonds, hydrazone bonds, or a combination of both. The 3 reaction pathways produce the self-assembly of the cage with yields ranging from 73% to 79%. Despite the complexity of the reaction the cage is formed in a very high yield, even for the reaction pathway that involves the formation of 16 bonds. This research paves the way for more sophisticated cage self-assembly designs.

Keywords: molecular cages; supramolecular chemistry; metal-organic cages; self-assembly

1. Introduction

Molecular cages are preorganized hosts with a central cavity that provides enhanced host–guest properties compared to less preorganized systems such as macrocycles [1,2], aiming to mimic the sophisticated cavity and functions of enzymes [3–6]. Chemists have developed synthetic methods to prepare both metal-organic cages and purely organic cages resulting in a wide range of structures with size- and shape-dependent host–guest properties [7–9]. Encapsulation in the cavity of cages results in different effects on the guest molecule, ranging from activation for catalytic reactions to protection from the surrounding media. These effects yielded multiple applications of molecular cages, including catalysis [10–15], sensing of chemicals [16–23], stabilization of chemical species [24,25], separation process [26–28], removal of pollutants from water [29–32] and biological applications [33–43] among many others [7,8,44,45].

The self-assembly of molecular cages from the constituent building block involves in most cases numerous reversible steps. Reversibility is key for error correction of improperly self-assembled by-products produced during the self-assembly process to give the final cage product [46–48]. For this, cage building blocks must have a specific shape and geometry that provides an appropriate preorganization in a similar fashion to macrocycles [7,49]. Besides the geometric requirements of the building blocks, both thermodynamic and kinetic are key in order to set up the appropriate reaction conditions, including concentration of reagents, reaction time, and temperature [46–48,50]. In this

 doi:10.20944/preprints202410.1100.v1

regard, computational modelling has been extensively used to design cages with specific geometries and properties such as predicting host-guest affinity [51–57].

Typically, metal-organic cages are prepared by the self-assembly reaction of ligands with metals forming metal–ligand bonds [8,58,59], and purely organic cages are prepared by the self-assembly reaction of ligands with complementary reactivity through reversible reactions such as imine and hydrazone bond formation [7,60,61]. There are examples of cages containing both metal–ligand bonds and reversible organic bonds, allowing their assembly via either type of bond, even both bonds simultaneously [8,62–64] Focusing in Pd(II) containing cages, the formation of Pd_2L_4 cages involves the self-assembly of two Pd(II) ions and four ditopic ligands, typically containing pyridine moieties [65–68], though Pd–pyridine coordination bonds [69]. Regarding hydrazone containing cages, hydrazone bonds are both reversible and robust [70], allowing the preparation of cages through the condensation reaction between hydrazide and aldehyde-containing building blocks [34,71–79]. Combining both strategies, Crowley and his team showed the feasibility of using simultaneously in the cage self-assembly both Pd–pyridine coordination bonds and hydrazone bonds [63], and we proved that it is possible to self-assemble cages that contain Pd–pyridine bonds through hydrazone bond formation [34]. These results open the way to explore multiple cage self-assembly reaction pathways involving both Pd–pyridine and hydrazone bonds. For this, we propose studying the self-assembly of a Pd_2L_4 cage through various reaction pathways involving the formation of Pd–ligand bonds, hydrazone bonds, or a combination of both.

In this work, we present a comparative study of the self-assembly of a Pd_2L_4 cage containing Pd–pyridine and hydrazone links [34]. The reversible nature of both bond types enables the self-assembly of the cage through the formation of Pd–ligand bonds or hydrazone bonds, utilizing three distinct reaction pathways (Figure 1). As far as we know, this is the first cage formation comparative study involving Pd–ligand and organic bond formation reactions. In particular, we focused on a Pd_2L_4 cage containing four dihydrazone units with a bended geometry and two $[PdPy_4]^{2+}$ units with a C_4 symmetric geometry that serve to cap the cage [34].

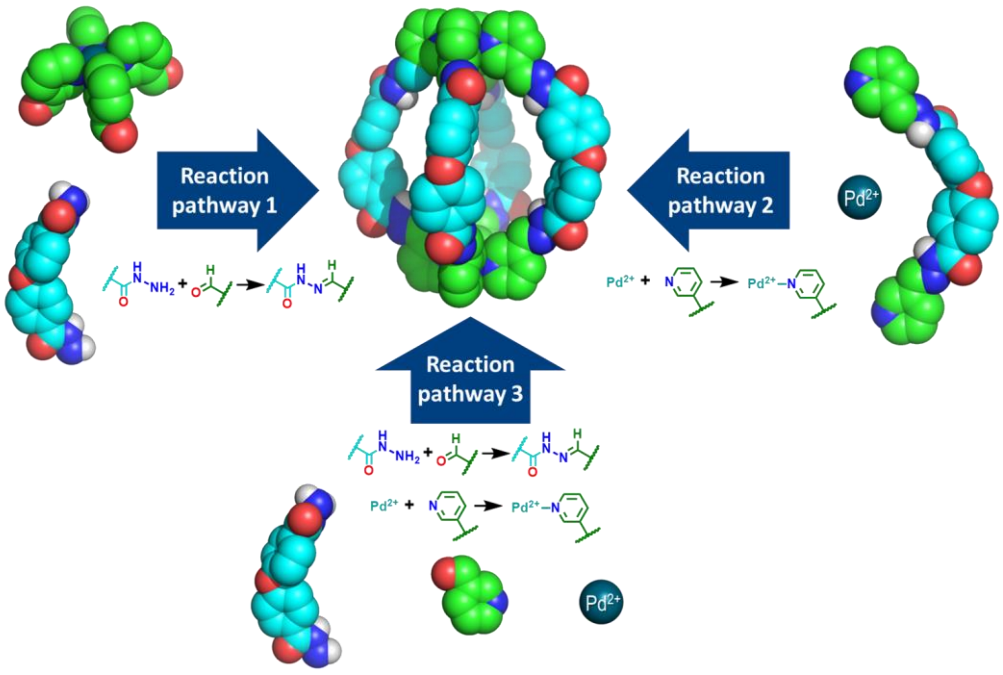

Figure 1. Schematic representation of the three reaction pathways for the self-assembly of a Pd_2L_4 cage containing hydrazone and Pd–pyridine bonds.

2. Results and Discussion

2.1. Self-Assembly Process of the PD_2L_4 Cage

Preprints.org (www.preprints.org) | NOT PEER-REVIEWED | Posted: 14 October 2024 doi:10.20944/preprints202410.1100.v1

The self-assembly of a Pd_2L_4 cage containing Pd–pyridine and hydrazone bonds can be performed through multiple ways. In this regard, we proposed 3 possible reactions to prepare the Pd_2L_4 cage **C1** (Figure 2). The reaction pathway 1 involves the reaction of dihydrazide ligand **1** and the square planar tetrapyridyl Pd^{2+} motif **2** by hydrazone bond formation [34]; the reaction pathway 2 comprises the reaction of dipyridine ligand **3** with Pd^{2+} by Pd–pyridine bond formation; and the reaction pathway 3 involves the reaction between dihydrazide ligand **1**, 3-pyridinecarboxaldehyde, and Pd^{2+} involving simultaneously Pd–pyridine and hydrazone bond formation. In all cases, the self-assembly of cage **C1** was performed in deuterated DMSO at 25 °C and formation was monitored by ^{1}H NMR spectroscopy. The solvent DMSO was chosen as it enables the complete solution of the reagents, cage, and reaction intermediates. Quantification of the concentration of the species in solution was performed by integration of the corresponding proton signals considering the concentration of the internal standard 1,4-dimethoxybenzene.

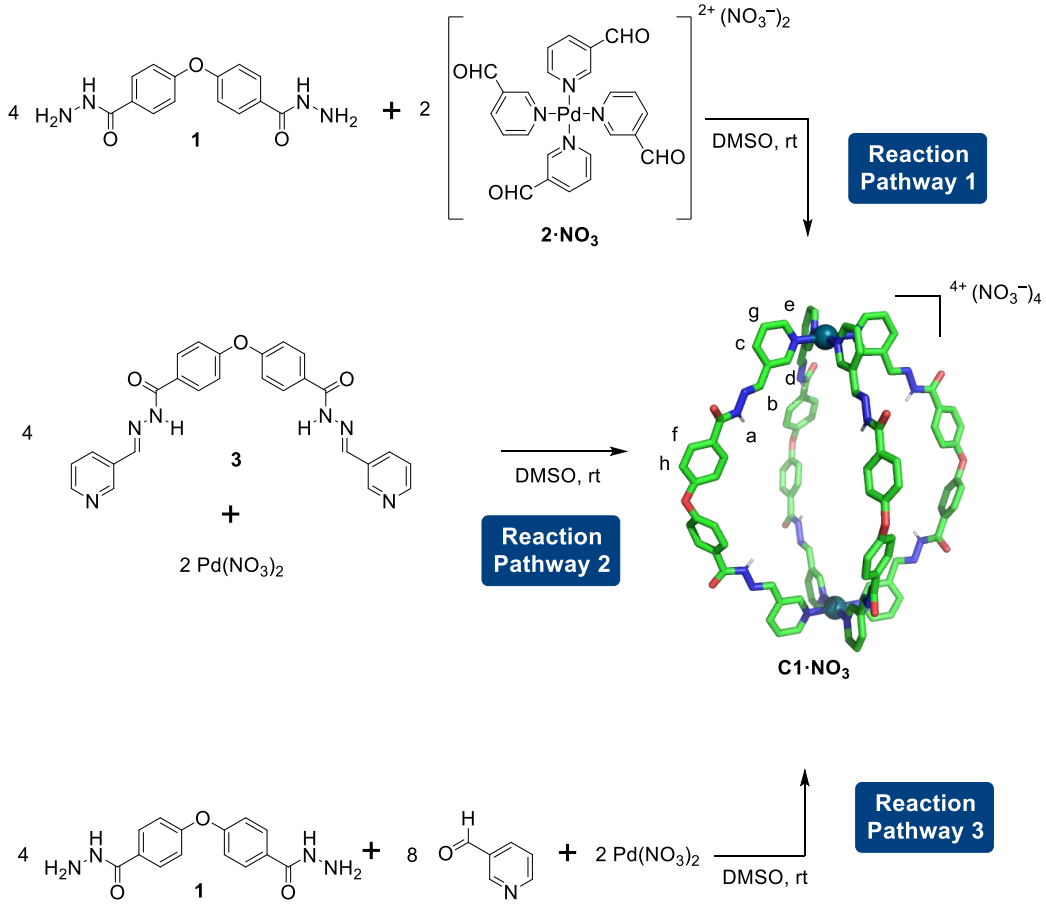

Figure 2. The three possible reaction pathways for the self-assembly of cage **C1** by Pd–pyridine and hydrazone bond formation. The lettering corresponds to the assignment of the ^{1}H NMR signals.

Initially we performed the self-assembly reaction of cage **C1** through reaction pathway 1. For this, we placed hydrazide **1** and tetrapyridyl–Pd^{2+} **2** in an NMR tube and monitored the evolution of the reaction by acquiring ^{1}H NMR spectra at different time intervals for a total of 55 hours (Figure 3). The signals corresponding to the starting materials disappeared rapidly with the simultaneous formation of the signals of the Pd_2L_4 cage. In contrast, few signals of the reaction intermediates could be observed in the reaction mixture, probably due to a combination of the formation of a large number of reaction intermediates in fast exchange with unsymmetrical structures containing chemically inequivalent NMR signals, as often observed in cage self-assembly reactions [46,80].

 doi:10.20944/preprints202410.1100.v1

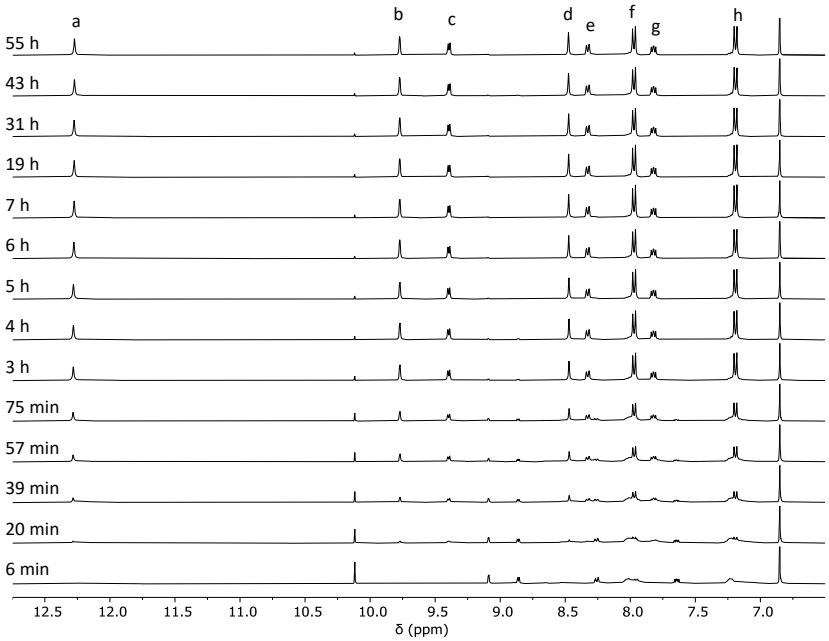

Figure 3. Evolution of the ^{1}H NMR (400 MHz, DMSO-d_6) of the self-assembly reaction of cage **C1** through reaction pathway 1 from **1** and **2**. The signal at 6.86 ppm corresponds to 1,4-dimethoxybenzene used as an internal standard. The assignment of cage signals is shown in Figure 2.

Then we performed the self-assembly reaction of cage **C1** through reaction pathway 2. We reacted hydrazide ligand **3** with $Pd(NO_3)_2$·to form the cage through Pd–pyridine bond formation. The reaction proceeds smoothly with the formation of cage **C1**, that is the only product observed in the ^{1}H NMR spectra (Figure 4). In contrast to reaction pathway 1, after 6 minutes, nearly all signals corresponding to the starting materials are absent, and the predominant signals in the spectra correspond to the cage. This highlights the rapid formation of the Pd–pyridine bonds, resulting in quick cage assembly.

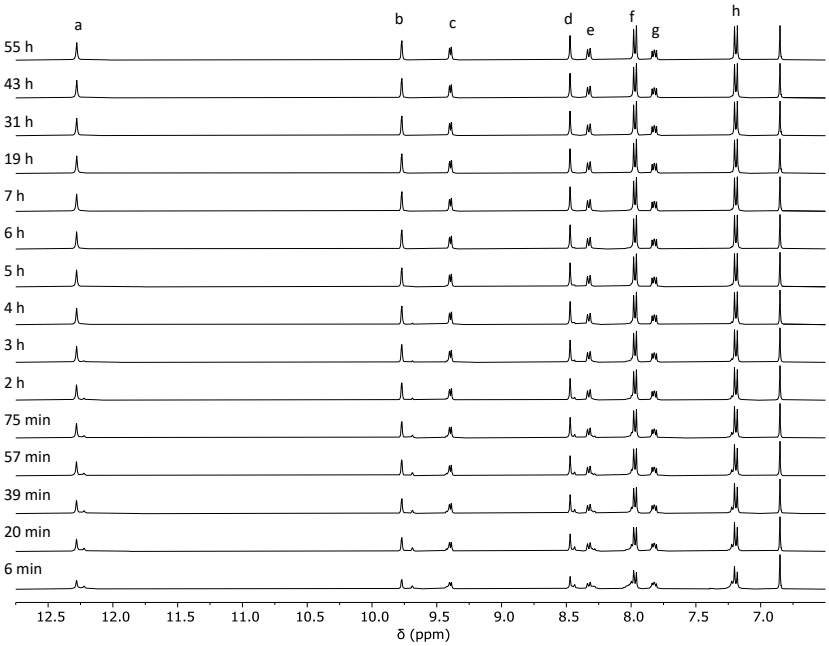

Figure 4. Evolution of the ^{1}H NMR (400 MHz, DMSO-d_6) of the self-assembly reaction of cage **C1** through reaction pathway 2 from **3** and $Pd(NO_3)_2$. The signal at 6.86 ppm corresponds to 1,4-

 doi:10.20944/preprints202410.1100.v1

dimethoxybenzene used as an internal standard. The assignment of cage signals is shown in Figure 2.

Finally, we performed the self-assembly reaction of cage **C1** through reaction pathway 3. This reaction is more complex, as it involves the simultaneous formation of 16 bonds, comprising 8 Pd–pyridine bonds and 8 hydrazone bonds. Indeed, this reaction pathway involves more difficulty, for example, the nitrogen atom of hydrazine **1** may result in competition with pyridine for Pd^{2+} coordination that may disturb the cage self-assembly pathway. However, despite this complexity, the reaction yields the expected **C1** cage in a clean self-assembly reaction (Figure 5). This self-assembly experiment highlights the feasibility of the simultaneous formation of Pd–pyridine and hydrazone bonds in a cage self-assembly reaction.

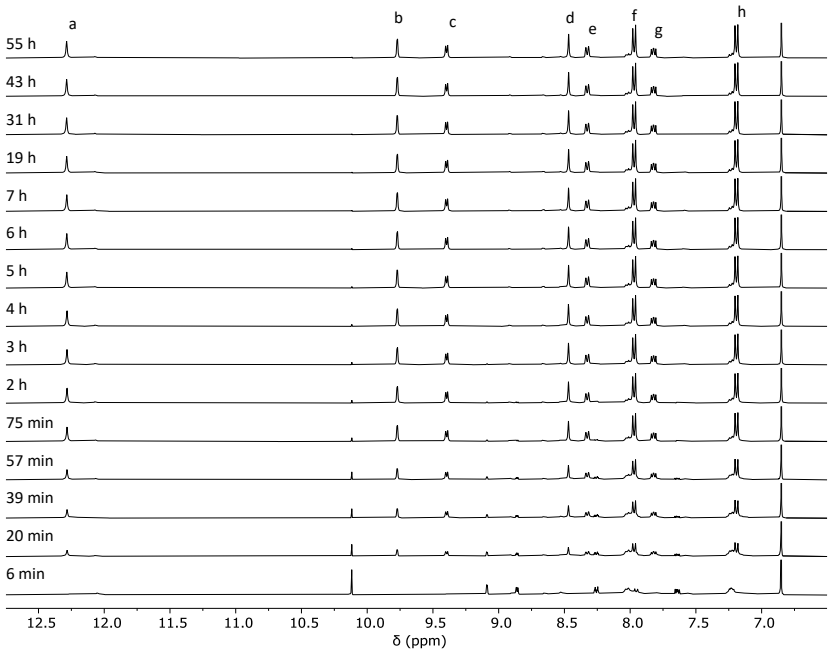

Figure 5. Evolution of the ^{1}H NMR (400 MHz, DMSO-d_6) of the self-assembly reaction of cage **C1** through reaction pathway 3 from **1**, $Pd(NO_3)_2$, and 3-pyridinecarboxaldehyde. The signal at 6.86 ppm corresponds to 1,4-dimethoxybenzene used as an internal standard. The assignment of cage signals is shown in Figure 2.

After performing the self-assembly reactions, we carried out a quantitative analysis of the integrals of the ^{1}H NMR signals for the three reaction pathways to evaluate the kinetics of cage formation. For this, the integral of the internal standard 1,4-dimethoxybenzene was taken into account (Figure 6). We observed that the fastest cage formation is for reaction pathway 2, which gives a 65% yield in 6 minutes. In contrast, reaction pathways 1 and 3, only give a 16% and 17% yield in 6 minutes, respectively. These results highlight that the formation of Pd–pyridine bond has a greater rate than the formation of hydrazone bond (reaction pathway 2 *vs.* reaction pathway 1). A key observation in reaction pathway 3, which involves the formation of 16 bonds through the self-assembly of 12 building blocks and 2 Pd(II) atoms, is that it exhibits similar reaction kinetics to pathway 1, which only requires the formation of 8 bonds from the self-assembly of 6 building blocks. This observation shows that hydrazone bond formation is the rate limiting step of the cage self-assembly process, in contrast to the fast Pd–pyridine bond formation. Focusing on the final cage formation yield at 55 hours of reaction, both reaction pathways 1 and 3 have similar yields in the range 78–79%, whereas reaction pathway 2 has a 73% yield. Despite all that, reaction pathway 2 is the fastest, the final yield is the lowest, highlighting that the final yield does not depend exclusively

 doi:10.20944/preprints202410.1100.v1

on the initial reaction rate. As the cage self-assembly yields are less than 100% for the three reaction pathways, in all three cases by-products are formed.

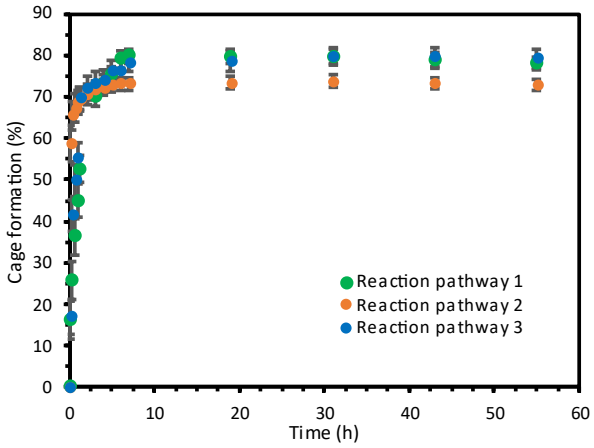

Figure 6. Evolution of the cage **C1** formation for the self-assembly reaction through reaction pathways 1 (green), 2 (orange), and 3 (blue). Cage formation yields have been determined by ^{1}H NMR using the integrals of the signals of the cage and 1,4-dimethoxybenzene which has been used as an internal standard.

In order to determine if the by-products formed in the three reaction pathways are visible by ^{1}H NMR, a close examination of the obtained spectra at the end of the reaction was performed. While reaction pathways 1 and 2 produce clean ^{1}H NMR spectra showing only the signals of cage **C1**, reaction pathway 3 displays a small set of additional peaks (Figure 7). This is probably due to the formation of asymmetric oligomeric structures possessing a number of chemically distinct NMR signals that are individually at too low a concentration to be observed by ^{1}H NMR.

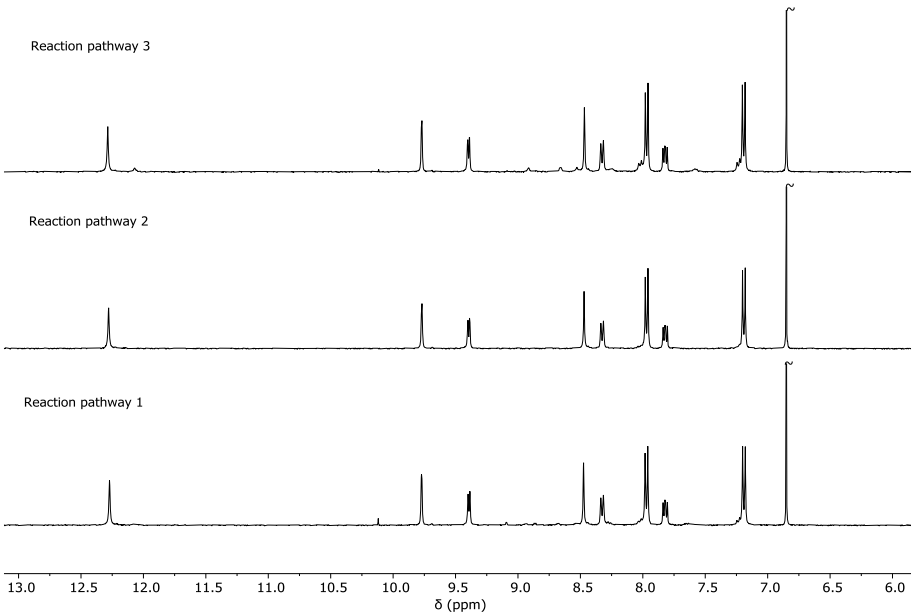

Figure 7. Comparison of the ^{1}H NMR obtained at 55 hours for the self-assembly reaction of cage **C1** through reaction pathways 1, 2, and 3. The signal at 6.86 ppm corresponds to 1,4-dimethoxybenzene used as an internal standard.

To understand the successful cage self-assembly observed in the three different reaction pathways, we additionally carried out molecular mechanics calculations. We performed a conformational search of the building blocks to obtain the most stable conformations. We observed that all conformations of ligands **1** and **3** have a bent configuration (Figure 8c,d), with good

 doi:10.20944/preprints202410.1100.v1

complementarity of ligand **1** to the geometry of metal complex **3** (Figure 8e) and ligand **3** to the square planar geometry of Pd(II). Specifically, the rigidity of the core Ph–O–Ph fragment of ligands **1** and **3** provides a key structural element with an average bent angle of 121 º (Figure 8c) and 118 º (Figure 8d), respectively. These angles match nicely the 130 ºC average angle the ligand has in the crystal structure of the cage **C1**·NO_3 (Figure 8a) and the theoretical angle of 120º of the chemical representation of cage **C1** (Figure 8b). This analysis suggests that the successful self-assembly of the ligands into the cage structure is linked to a favorable preorganization of the building blocks, whose geometry aligns well with the cage structure.

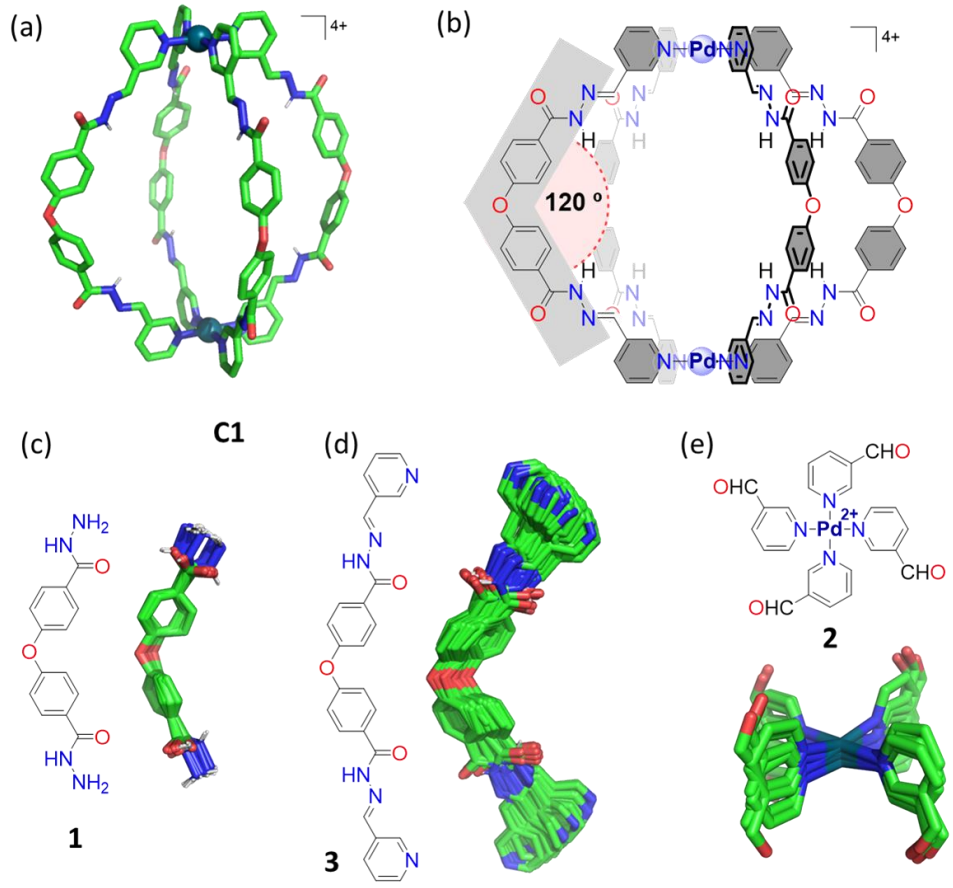

Figure 8. (a) Crystal structure of cage **C1**·NO_3 (CCDC 2295536).[34] (b) Chemical representation of the structure of cage **C1** highlighting the ideal 120 º angle of the ligand. (c–e) A conformational search performed at MMFF level of theory using the software Wavefunction Spartan 20 (overlay of the found conformers in a 2 kcal/mol energy window).

3. Materials and Methods

Materials. All chemicals and solvents were obtained from commercial sources and used without further purification unless specified.

NMR Experiments. ^{1}H spectra were recorded on a Bruker FT-NMR Avance 400 (Ettlingen, Germany) spectrometer at 300K. Chemical shifts (δ) are reported in parts per million (ppm) and referenced to residual solvent peak.

Molecular Modelling. The structure of ligands was modelled with the Spartan' 20 software, using the built-in conformational search algorithm using the MMFF force field [81].

3.1. Synthesis of Ligands and Cages

Compounds **1**, **2**, **3**, and **C1** were prepared as described by our research group as reported in the literature [34].

 doi:10.20944/preprints202410.1100.v1

3.2. Cage Formation Kinetic Experiments

All ^{1}H NMR kinetic experiments were performed using the following general procedure. To an NMR tube was introduced **1** (2.6 mg, 9.2 μmol) and **2** (3.0 mg, 4.6 μmol) for reaction pathway 1; **3** (4.3 mg, 9.2 μmol) and $Pd(NO_3)_2{\cdot}2H_2O$ (1.2 mg, 4.6 μmol) for reaction pathway 2; or **1** (2.6 mg, 9.2 μmol), and $Pd(NO_3)_2{\cdot}2H_2O$ (1.2 mg, 4.6 μmol) for reaction pathway 3. Then a stock solution of 1,4-dimethoxybenzene as internal standard in DMSO-d_6 (600 μL of a 10 mM stock solution) was added for reaction pathways 1 and 2. For reaction pathway 3 a solution of 1,4-dimethoxybenzene as internal standard (600 μL of a 10 mM stock solution) containing 3-pyridinecarboxaldehyde (1.8 μL, 18.4 mmol). The reaction was shaken to get a clear solution of all the components and the crude reaction mixture was monitored by ^{1}H NMR for 55 hours at 25 ºC. The concentration of all chemical species was determined for each reaction time by the analysis of integrals of the ^{1}H NMR signals of the cage and the internal standard, reporting the yield as the average. All reactions were performed at least twice, and a representative example is reported in the manuscript.

5. Conclusions

We have performed a study of the self-assembly of a Pd_2L_4 hydrazone molecular cage **C1** through 3 different reaction pathways involving formation of Pd–ligand bonds, hydrazone bonds, or a combination of both. Our results show that it is possible to self-assemble the cage structure **C1** through 3 different reaction pathways, obtaining yields ranging from 73 to 79%, with the lowest yield observed for pathway 2 (73%) and similar yields for pathways 1 and 3 (78% and 79%, respectively). The fastest initial reaction rate is observed for reaction pathway 2, compared to reaction pathways 1 and 3, that have similar initial reaction rates, indicating that Pd-pyridine bonds are formed faster than hydrazone bonds. In overall, the self-assembly reaction pathway influences the initial reaction kinetics and the final cage yield. We also proved that despite the complexity of the reaction pathway 3, that involves the formation of 16 bonds in contrast to reaction pathways 1 and 2 that only involve the formation of 8 bonds, the cage is formed in a 79% yield. Molecular modelling shows that the ligands have a favorable reorganization, whose geometry matches well with the cage structure. We anticipate that these results will open the way for more complex cage self-assembly designs involving the simultaneous formation of both Pd–ligand and hydrazone bonds.

Supplementary Materials: The following supporting information can be downloaded at: www.mdpi.com/xxx/s1, Supporting Information (PDF file).

Author Contributions: Conceptualization, V.M-C.; methodology, G.M.-G.; experiments, G.M.-G.; writing—original draft preparation, G.M.-G., V.M-C. and R.M-.M.; writing—review and editing, G.M.-G., V.M-C. and R.M-.M.; supervision, V.M-C. and R.M-.M.; project administration, V.M-C. and R.M-.M.; funding acquisition, V.M-C. and R.M-.M. All authors have read and agreed to the published version of the manuscript.

Funding: V. M.-C. acknowledges the financial support from project CIDEGENT/2020/031 funded by the Generalitat Valenciana, project PID2020-113256RA-I00 funded by MICIU/AEI/10.13039/501100011033, and project CNS2023-144879 funded by MICIU/AEI/10.13039/501100011033 and European Union NextGenerationEU/PRTR. R. M.-M. acknowledges the financial support from project PROMETEO CIPROM/2021/007 from the Generalitat Valenciana and project PID2021-126304OB-C41 funded by MICIU/AEI/10.13039/501100011033 and FEDER A way to make Europe.

Data Availability Statement: The original contributions presented in the study are included in the article/supplementary material, further inquiries can be directed to the corresponding author/s.

Acknowledgments: U26 facility of ICTS "NANBIOSIS" is acknowledged for support in the NMR characterization of compounds. This research was supported by CIBER (CB06/01/2012), Instituto de Salud Carlos III, Ministerio de Ciencia e Innovación.

Conflicts of Interest: The authors declare no conflicts of interest.

References

1. Martí-Centelles, V.; Duarte, F.; Lusby, P. J. Host-Guest Chemistry of Self-Assembled Hemi-Cage Systems: The Dramatic Effect of Lost Pre-Organization. *Isr. J. Chem.* **2019**, *59*, 257–266. https://doi.org/10.1002/ijch.201800
2. Rondelli, M.; Daranas, A. H.; Martín, T. Importance of Precursor Adaptability in the Assembly of Molecular Organic Cages. *J. Org. Chem.* **2023**, *88* (4), 2113–2121. https://doi.org/10.1021/acs.joc.2c02523
3. Lewis, J. E. M. Developing Sophisticated Microenvironments in Metal-organic Cages. *Trends Chem.* **2023**, *5* (10), 717–719. https://doi.org/10.1016/j.trechm.2023.06.003
4. Barber, B. E.; Jamieson, E. M. G.; White, L. E. M.; McTernan, C. T. Metal-Peptidic Cages—Helical Oligoprolines Generate Highly Anisotropic Nanospaces with Emergent Isomer Control. *Chem* **2024**, *10* (9), 2792–2806. https://doi.org/10.1016/j.chempr.2024.05.002
5. Yuan, J.; Guan, Z.; Lin, H.; Yan, B.; Liu, K.; Zhou, H.; Fang, Y. Modeling the Enzyme Specificity by Molecular Cages Through Regulating Reactive Oxygen Species Evolution. *Angew. Chem. Int. Ed.* **2023**, *62* (31), e202303896. https://doi.org/10.1002/anie.202303896
6. Bhattacharyya, S.; Ali, S. R.; Venkateswarulu, M.; Howlader, P.; Zangrando, E.; De, M.; Mukherjee, P. S. Self-Assembled Pd_{12} Coordination Cage as Photoregulated Oxidase-Like Nanozyme. *J. Am. Chem. Soc.* **2020**, *142* (44), 18981–18989. https://doi.org/10.1021/jacs.0c09567
7. Montà-González, G.; Sancenón, F.; Martínez-Máñez, R.; Martí-Centelles, V. Purely Covalent Molecular Cages and Containers for Guest Encapsulation. *Chem. Rev.* **2022**, *122* (16), 13636–13708. https://doi.org/10.1021/acs.chemrev.2c00198
8. Percástegui, E. G.; Ronson, T. K.; Nitschke, J. R. Design and Applications of Water-soluble Coordination Cages. *Chem. Rev.* **2020**, *120* (24), 13480–13544. https://doi.org/10.1021/acs.chemrev.0c00672
9. Cox, C. J. T.; Hale, J.; Molinska, P.; Lewis, J. E. M. Supramolecular and Molecular Capsules, Cages, and Containers. *Chem. Soc. Rev.* **2024**, ASAP. https://doi.org/10.1039/D4CS00761A
10. Martí-Centelles, V.; Lawrence, A. L.; Lusby, P. J. High Activity and Efficient Turnover by a Simple, Self-Assembled Artificial "Diels-Alderase". *J. Am. Chem. Soc.* **2018**, *140*, 2862–2868. https://doi.org/10.1021/jacs.7b12146
11. Yu, Y.; Yang, J. M.; Rebek, J. Molecules in Confined Spaces: Reactivities and Possibilities in Cavitands. *Chem.* **2020**, *6*, 1265– 1274. https://doi.org/10.1016/j.chempr.2020.04.014
12. Pappalardo, A.; Puglisi, R.; Trusso Sfrazzetto, G. Catalysis inside Supramolecular Capsules: Recent Developments. *Catalysts* **2019**, *9*, 630. https://doi.org/10.3390/catal9070630
13. Chen, S.; Chen, L.-J. Metal–organic Cages: Applications in Organic Reactions. *Chemistry* **2022**, *4* (2), 494–519. https://doi.org/10.3390/chemistry4020036
14. Piskorz, T. K.; Martí-Centelles, V.; Spicer, R. L.; Duarte, F.; Lusby, P. J. Picking the Lock of Coordination Cage Catalysis. *Chem. Sci.* **2023**, *14*, 11300–11331. https://doi.org/10.1039/D3SC02586A
15. Chen, S.; Chen, L.-J. Metal–Organic Cages: Applications in Organic Reactions. *Chemistry* **2022**, *4*, 494–519. https://doi.org/10.3390/chemistry4020036
16. Luo, K.; Liu, Y.; Li, A.; Lai, Z.; Long, Z.; He, Q. A Tetraphenylethylene-Based Superphane for Selective Detection and Adsorption of Trace Picric Acid in Aqueous Media. *Supramol. Chem.* **2024**, 1–10. https://doi.org/10.1080/10610278.2024.2398575
17. La Cognata, S.; Amendola, V. Recent Applications of Organic Cages in Sensing and Separation Processes in Solution. *Chem. Commun.* **2023**, *59*, 13668–13678. https://doi.org/10.1039/D3CC04522F
18. Merli, D.; La Cognata, S.; Balduzzi, F.; Miljkovic, A.; Toma, L.; Amendola, V. A Smart Supramolecular Device for the Detection of *t,t*-Muconic Acid in Urine. *New J. Chem.* **2018**, *42*, 15460–15465. https://doi.org/10.1039/C8NJ02156B
19. Ludden, M. D.; Taylor, C. G. P.; Ward, M. D. Orthogonal Binding and Displacement of Different Guest Types Using a Coordination Cage Host with Cavity-Based and Surface-Based Binding Sites. *Chem. Sci.* **2021**, *12*, 12640–12650. https://doi.org/10.1039/D1SC04272F
20. Lu, Y.; Wang, S.-M.; He, S.-S.; Huang, Q.; Zhao, C.-D.; Yu, S.; Jiang, W.; Yao, H.; Wang, L.-L.; Yang, L.-P. An Endo-functionalized Molecular Cage for Selective Potentiometric Determination of Creatinine. *Chem. Sci.* **2024**, *14*, 14791–14797. https://doi.org/10.1039/d4sc04950k
21. Luo, K.; Liu, Y.; Li, A.; Lai, Z.; Long, Z.; He, Q. A Tetraphenylethylene-Based Superphane for Selective Detection and Adsorption of Trace Picric Acid in Aqueous Media. *Supramol. Chem.* **2024**, 1–10. https://doi.org/10.1080/10610278.2024.2398575
22. Lu, Y.; Wang, S.-M.; He, S.-S.; Huang, Q.; Zhao, C.-D.; Yu, S.; Jiang, W.; Yao, H.; Wang, L.-L.; Yang, L.-P. An Endo-functionalized Molecular Cage for Selective Potentiometric Determination of Creatinine. *Chem. Sci.* **2024**, *15* (36), 14791–14797. https://doi.org/10.1039/d4sc04950k

23. Maitra, P. K.; Bhattacharyya, S.; Purba, P. C.; Mukherjee, P. S. Coordination-induced Emissive Poly-nhc-derived Metallacage for Pesticide Detection. *Inorg. Chem.* **2024**, *63* (5), 2569–2576. https://doi.org/10.1021/acs.inorgchem.3c03759
24. Mal, P.; Breiner, B.; Rissanen, K.; Nitschke, J. R. White Phosphorus is Air-Stable within a Self-Assembled Tetrahedral Capsule. *Science* **2009**, *324*(5935), 1697-1699. https://doi.org/10.1126/science.1175313
25. Galan, A.; Ballester, P. Stabilization of Reactive Species by Supramolecular Encapsulation. *Chem. Soc. Rev.* **2016**, *45*, 1720– 1737. https://doi.org/10.1039/C5CS00861A
26. Zhang, D.; Ronson, T. K.; Zou, Y.-Q.; Nitschke, J. R. Metal–organic Cages for Molecular Separations. *Nat. Rev. Chem.* **2021**, *5* (3), 168–182. https://doi.org/10.1038/s41570-020-00246-1
27. Little, M. A.; Cooper, A. I. The Chemistry of Porous Organic Molecular Materials. *Adv. Funct. Mater.* **2020**, *30*, 1909842. https://doi.org/10.1002/adfm.201909842
28. Zhang, J.; Xie, S.; Zi, M.; Yuan, L. Recent Advances of Application of Porous Molecular Cages for Enantioselective Recognition and Separation. *J. Sep. Sci.* **2020**, *43* (1), 134–149. https://doi.org/10.1002/jssc.201900762
29. Pérez-Ferreiro, M.; Gallagher, Q. M.; León, A. B.; Webb, M. A.; Criado, A.; Mosquera, J. Engineering a Surfactant Trap via Postassembly Modification of an Imine Cage. *Chem. Mater.* **2024**, *36*, 8920–8928. https://doi.org/10.1021/acs.chemmater.4c01808
30. Wang, Z.; Pacheco-Fernández, I.; Carpenter, J. E.; Aoyama, T.; Huang, G.; Pournaghshband Isfahani, A.; Ghalei, B.; Sivaniah, E.; Urayama, K.; Colón, Y. J.; Furukawa, S. Pore-networked Membrane Using Linked Metal-organic Polyhedra for Trace-level Pollutant Removal and Detection in Environmental Water. *Commun. Mater.* **2024**, *5* (1), 161. https://doi.org/10.1038/s43246-024-00607-z
31. Samanta, J.; Tang, M.; Zhang, M.; Hughes, R. P.; Staples, R. J.; Ke, C. Tripodal Organic Cages with Unconventional CH···O Interactions for Perchlorate Remediation in Water. *J. Am. Chem. Soc.* **2023**, *145* (40), 21723–21728. https://doi.org/10.1021/jacs.3c06379
32. Liu, X.; Zhang, Z.; Shui, F.; Zhang, S.; Li, L.; Wang, J.; Yi, M.; You, Z.; Yang, S.; Yang, R.; Wang, S.; Liu, Y.; Zhao, Q.; Li, B.; Bu, X.; Ma, S. Porous Organic Cage as an Efficient Platform for Industrial Radioactive Iodine Capture. *Angew. Chem. Int. Ed.* **2024**, e202411342. https://doi.org/10.1002/anie.202411342
33. Montà-González, G.; Ortiz-Gómez, E.; López-Lima, R.; Fiorini, G.; Martínez-Máñez, R.; Martí-Centelles, V. Water-Soluble Molecular Cages for Biological Applications. *Molecules* **2024**, *29*(7), 1621; https://doi.org/10.3390/molecules29071621
34. Montà-González, G.; Bastante-Rodríguez, D.; García-Fernández, A.; Lusby, P. J.; Martínez-Máñez, R.; Martí-Centelles, V. Comparing organic and metallo-organic hydrazone molecular cages as potential carriers for doxorubicin delivery. *Chem. Sci.* **2024**, *15*(26), 10010–10017. https://doi.org/10.1039/D4SC02294G
35. Casini, A.; Woods, B.; Wenzel, M. The Promise of Self-Assembled 3D Supramolecular Coordination Complexes for Biomedical Applications. *Inorg. Chem.* **2017**, *56*, 14715–14729. https://doi.org/10.1021/acs.inorgchem.7b02599
36. Zhu, C.-Y.; Pan, M.; Su, C.-Y. Metal-Organic Cages for Biomedical Applications. *Isr. J. Chem.* **2018**, *59* (3-4), 209-219, https://doi.org/10.1002/ijch.201800147
37. Dou, W.-T.; Yang, C.-Y.; Hu, L.-R.; Song, B.; Jin, T.; Jia, P.-P.; Ji, X.; Zheng, F.; Yang, H.-B.; Xu, L. Metallacages and Covalent Cages for Biological Imaging and Therapeutics. *ACS Mater. Lett.* **2023**, *5* (4), 1061–1082. https://doi.org/10.1021/acsmaterialslett.2c01147
38. Ahmad, N.; Younus, H. A.; Chughtai, A. H.; Verpoort, F. Metal–organic Molecular Cages: Applications of Biochemical Implications. *Chem. Soc. Rev.* **2015**, *44* (1), 9–25. https://doi.org/10.1039/c4cs00222a
39. Sun, D.; Feng, X.; Zhu, X.; Wang, Y.; Yang, J. Anticancer Agents Based on Metal Organic Cages. *Coord. Chem. Rev.* **2024**, *500*, 215546. https://doi.org/10.1016/j.ccr.2023.215546
40. Cruz-Nava, S.; De Jesús Valencia-Loza, S.; Percástegui, E. G. Protection and Transformation of Natural Products Within Aqueous Metal-organic Cages. *Eur. J. Org. Chem.* **2022**, *2022* (40), e202200844. https://doi.org/10.1002/ejoc.202200844
41. Tapia, L.; Alfonso, I.; Solà, J. Molecular Cages for Biological Applications. *Org. Biomol. Chem.* **2021**, *19*(44), 9527–9540. https://doi.org/10.1039/d1ob01737c
42. Tapia, L.; Pérez, Y.; Carreira-Barral, I.; Bujons, J.; Bolte, M.; Bedia, C.; Solà, J.; Quesada, R.; Alfonso, I. Tuning pH-dependent Cytotoxicity in Cancer Cells by Peripheral Fluorine Substitution on Pseudopeptidic Cages. *Cell Rep. Phys. Sci.* **2024**, 102152. https://doi.org/10.1016/j.xcrp.2024.102152
43. Montà-González, G.; Martínez-Máñez, R.; Martí-Centelles, V. Requirements of Constrictive Binding and Dynamic Systems on Molecular Cages for Drug Delivery. *Preprints* **2024**, 2024100823. https://doi.org/10.20944/preprints202410.0823.v1
44. Zhang, G.; Mastalerz, M. Organic Cage Compounds-from Shape-Persistency to Function. *Chem. Soc. Rev.* **2014**, *43*, 1934–1947. https://doi.org/10.1039/C3CS60358J
45. Liu, W.; Stoddart, J. F. Emergent Behavior in Nanoconfined Molecular Containers. *Chem.* **2021**, *7*, 919–947. https://doi.org/10.1016/j.chempr.2021.02.016

46. Kai, S.; Martí-Centelles, V.; Sakuma, Y.; Mashiko, T.; Kojima, T.; Nagashima, U.; Tachikawa, M.; Lusby, P. J.; Hiraoka, S. Quantitative Analysis of Self-Assembly Process of a Pd_2L_4 Cage Consisting of Rigid Ditopic Ligands. *Chem. Eur. J.* **2018**, *24*(3), 663–671. https://doi.org/10.1002/chem.201704285
47. Abe, T.; Sanada, N.; Takeuchi, K.; Okazawa, A.; Hiraoka, S. Assembly of Six Types of Heteroleptic Pd_2L_4 Cages Under Kinetic Control. *J. Am. Chem. Soc.* **2023**, *145* (51), 28061–28074. https://doi.org/10.1021/jacs.3c09359
48. Foianesi-Takeshige, L. H.; Takahashi, S.; Tateishi, T.; Sekine, R.; Okazawa, A.; Zhu, W.; Kojima, T.; Harano, K.; Nakamura, E.; Sato, H.; Hiraoka, S. Bifurcation of Self-assembly Pathways to Sheet or Cage Controlled by Kinetic Template Effect. *Commun. Chem.* **2019**, *2* (1). https://doi.org/10.1038/s42004-019-0232-2
49. Martí-Centelles, V.; Pandey, M. D.; Burguete, M. I.; Luis, S. V. Macrocyclization Reactions: The Importance of Conformational, Configurational, and Template-Induced Preorganization. *Chem. Rev.* **2015**, *115*(16), 8736–8834. https://doi.org/10.1021/acs.chemrev.5b00056
50. Martí-Centelles, V. Kinetic and thermodynamic concepts as synthetic tools in supramolecular chemistry for preparing macrocycles and molecular cages. *Tetrahedron Lett.* **2022**, *93*, 153676. https://doi.org/10.1016/j.tetlet.2022.153676
51. Martí-Centelles, V.; Piskorz, T. K.; Duarte, F. CageCavityCalc (*C3*): A Computational Tool for Calculating and Visualizing Cavities in Molecular Cages. *J. Chem. Inf. Model.* **2024**, *64* (14), 5604–5616. https://doi.org/10.1021/acs.jcim.4c00355
52. Piskorz, T. K.; Martí-Centelles, V.; Young, T. A.; Lusby, P. J.; Duarte, F. Computational Modeling of Supramolecular Metallo-organic Cages-Challenges and Opportunities. *ACS Catal.* **2022**, *12* (10), 5806–5826. https://doi.org/10.1021/acscatal.2c00837
53. Tarzia, A.; Wolpert, E. H.; Jelfs, K. E.; Pavan, G. M. Systematic Exploration of Accessible Topologies of Cage Molecules via Minimalistic Models. *Chem. Sci.* **2023**, *14* (44), 12506–12517. https://doi.org/10.1039/d3sc03991a
54. Young, T. A.; Gheorghe, R.; Duarte, F. cgbind: A Python Module and Web App for Automated Metallocage Construction and Host–Guest Characterization. *J. Chem. Inf. Model.* **2020**, *60* (7), 3546–3557. https://doi.org/10.1021/acs.jcim.0c00519
55. Turcani, L.; Tarzia, A.; Szczypiński, F. T.; Jelfs, K. E. stk: An Extendable Python Framework for Automated Molecular and Supramolecular Structure Assembly and Discovery. *J. Chem. Phys.* **2021**, *154* (21), 214102. https://doi.org/10.1063/5.0049708
56. Santolini, V.; Miklitz, M.; Berardo, E.; Jelfs, K. E. Topological Landscapes of Porous Organic Cages. *Nanoscale* **2017**, *9* (16), 5280–5298. https://doi.org/10.1039/c7nr00703e
57. Greenaway, R. L.; Jelfs, K. E. High-throughput Approaches for the Discovery of Supramolecular Organic Cages. *ChemPlusChem* **2020**, *85* (8), 1813–1823. https://doi.org/10.1002/cplu.202000445
58. Mcconnell, A. J. Metallosupramolecular Cages: From Design Principles and Characterisation Techniques to Applications. *Chem. Soc. Rev.* **2022**, *51* (8), 2957–2971. https://doi.org/10.1039/d1cs01143j
59. Cook, T. R.; Stang, P. J. Recent Developments in the Preparation and Chemistry of Metallacycles and Metallacages via Coordination. *Chem. Rev.* **2015**, *115* (15), 7001–7045. https://doi.org/10.1021/cr5005666
60. Xu, Z.; Ye, Y.; Liu, Y.; Liu, H.; Jiang, S. Design and Assembly of Porous Organic Cages. *Chem. Commun.* **2024**, *60* (17), 2261–2282. https://doi.org/10.1039/d3cc05091b
61. Yang, X.; Ullah, Z.; Stoddart, J. F.; Yavuz, C. T. Porous Organic Cages. *Chem. Rev.* **2023**, *123* (8), 4602–4634. https://doi.org/10.1021/acs.chemrev.2c00667
62. Van Hilst, Q. V. C.; Pearcy, A. C.; Preston, D.; Wright, L. J.; Hartinger, C. G.; Brooks, H. J. L.; Crowley, J. D. A Dynamic Covalent Approach to $[Pt_nL_{2n}]^{2n+}$ Cages. *Chem. Commun.* **2024**, *60* (32), 4302–4305. https://doi.org/10.1039/d4cc00323c
63. Lisboa, L. S.; Riisom, M.; Dunne, H. J.; Preston, D.; Jamieson, S. M. F.; Wright, L. J.; Hartinger, C. G.; Crowley, J. D. Hydrazone- and Imine-containing $[PdPtL_4]^{4+}$ Cages: A Comparative Study of the Stability and Host–guest Chemistry. *Dalton Trans.* **2022**, *51* (48), 18438–18445. https://doi.org/10.1039/d2dt02720h
64. Pradhan, S.; John, R. P. Self-assembled Pd6l4 Cage and Pd4l4 Square Using Hydrazide Based Ligands: Synthesis, Characterization and Catalytic Activity in Suzuki–Miyaura Coupling Reactions. *RSC Adv.* **2016**, *6* (15), 12453–12460. https://doi.org/10.1039/c6ra00055j
65. Han, M.; Engelhard, D. M.; Clever, G. H. Self-assembled Coordination Cages Based on Banana-shaped Ligands. *Chem. Soc. Rev.* **2014**, *43* (6), 1848–1860. https://doi.org/10.1039/c3cs60473j
66. Pullen, S.; Tessarolo, J.; Clever, G. H. Increasing Structural and Functional Complexity in Self-assembled Coordination Cages. *Chem. Sci.* **2021**, *12* (21), 7269–7293. https://doi.org/10.1039/d1sc01226f
67. Moree, L. K.; Faulkner, L. A. V.; Crowley, J. D. Heterometallic Cages: Synthesis and Applications. *Chem. Soc. Rev.* **2024**, *53* (1), 25–46. https://doi.org/10.1039/d3cs00690e
68. Schmidt, A.; Casini, A.; Kühn, F. E. Self-Assembled M_2L_4 Coordination Cages: Synthesis and Potential Applications. *Coord. Chem. Rev.* **2014**, *275*, 19–36. https://doi.org/10.1016/j.ccr.2014.03.037

69. Kurpik, G.; Walczak, A.; Gołdyn, M.; Harrowfield, J.; Stefankiewicz, A. R. Pd(II) Complexes with Pyridine Ligands: Substituent Effects on the NMR Data, Crystal Structures, and Catalytic Activity. *Inorg. Chem.* **2022**, *61* (35), 14019–14029. https://doi.org/10.1021/acs.inorgchem.2c01996
70. Nguyen, R.; Huc, I. Optimizing the Reversibility of Hydrazone Formation for Dynamic Combinatorial Chemistry. *Chem. Commun.* **2003**, 942–943. https://doi.org/10.1039/b211645f
71. Lin, Z.; Emge, T. J.; Warmuth, R. Multicomponent Assembly of Cavitand-based Polyacylhydrazone Nanocapsules. *Chem. Eur. J.* **2011**, *17* (34), 9395–9405. https://doi.org/10.1002/chem.201100527
72. Wierzbicki, M.; Głowacka, A. A.; Szymański, M. P.; Szumna, A. A Chiral Member of the Family of Organic Hexameric Cages. *Chem. Commun.* **2017**, *53* (37), 5200–5203. https://doi.org/10.1039/c7cc02245j
73. Yang, M.; Qiu, F.; M. El-Sayed, E.-S.; Wang, W.; Du, S.; Su, K.; Yuan, D. Water-stable Hydrazone-linked Porous Organic Cages. *Chem. Sci.* **2021**, *12* (40), 13307–13315. https://doi.org/10.1039/d1sc04531h
74. Foyle, E.; Mason, T.; Coote, M.; Izgorodina, E.; White, N. Robust Organic Cages Prepared Using Hydrazone Condensation Display Sulfate/hydrogenphosphate Selectivity in Water. *ChemRxiv*, **2024**. https://doi.org/10.26434/chemrxiv-2021-qqhs8
75. Zheng, X.; Zhang, Y.; Wu, G.; Liu, J.-R.; Cao, N.; Wang, L.; Wang, Y.; Li, X.; Hong, X.; Yang, C.; Li, H. Temperature-dependent Self-assembly of a Purely Organic Cage in Water. *Chem. Commun.* **2018**, *54* (25), 3138–3141. https://doi.org/10.1039/c8cc01085d
76. Xu, Y.-Y.; Liu, H.-K.; Wang, Z.-K.; Song, B.; Zhang, D.-W.; Wang, H.; Li, Z.; Li, X.; Li, Z.-T. Olive-shaped Organic Cages: Synthesis and Remarkable Promotion of Hydrazone Condensation Through Encapsulation in Water. *J. Org. Chem.* **2021**, *86* (5), 3943–3951. https://doi.org/10.1021/acs.joc.0c02792
77. Vestrheim, O.; Schenkelberg, M. E.; Dai, Q.; Schneebeli, S. T. Efficient Multigram Procedure for the Synthesis of Large Hydrazone-linked Molecular Cages. *Org. Chem. Front.* **2023**, *10* (16), 3965–3974. https://doi.org/10.1039/d3qo00480e
78. Foyle, É. M.; Goodwin, R. J.; Cox, C. J. T.; Smith, B. R.; Colebatch, A. L.; White, N. G. Expedient Decagram-Scale Synthesis of Robust Organic Cages That Bind Sulfate Strongly and Selectively in Water. *J. Am. Chem. Soc.* **2024**, *146* (39), 27127–27137. https://doi.org/10.1021/jacs.4c09930
79. Cortón, P.; Wang, H.; Neira, I.; Blanco-Gómez, A.; Pazos, E.; Peinador, C.; Li, H.; García, M. D. "The Red Cage": Implementation of Ph-responsiveness Within a Macrobicyclic Pyridinium-based Molecular Host. *Org. Chem. Front.* **2022**, *9* (1), 81–87. https://doi.org/10.1039/d1qo01331a
80. Hiraoka, S. Self-Assembly Processes of Pd(II)- and Pt(II)-Linked Discrete Self-Assemblies Revealed by QASAP. *Isr. J. Chem.* **2019**, *59* (3-4), 151–165. https://doi.org/10.1002/ijch.201800073
81. Deppmeier, B. J.; Driessen, A. J.; Hehre, T. S.; Hehre, W. J.; Johnson, J. A.; Klunzinger, P. E.; Leonard, J. M.; Pham, I. N.; Pietro, W. J.;Jianguo, Y. Spartan '20, version 1.0.0 (Mar 8th 2021),Wavefunction Inc., 2011.